Symmetric and asymmetric optical multipeak solitons on a continuous wave background in the femtosecond regime

Chong Liu,[1,2,*] Zhan-Ying Yang,[1,2,†] Li-Chen Zhao,[1,2] Liang Duan,[1,2] Guangye Yang,[3] and Wen-Li Yang[2,4]

[1]*School of Physics, Northwest University, Xi'an 710069, China*

[2]*Shaanxi Key Laboratory for Theoretical Physics Frontiers, Xi'an 710069, China*

[3]*Department of Physics, Shanxi Medical University, Taiyuan, Shanxi 030001, China*

[4]*Institute of Modern Physics, Northwest University, Xi'an 710069, China*

(Received 8 May 2016; published 25 October 2016)

We study symmetric and asymmetric optical multipeak solitons *on a continuous wave background* in the femtosecond regime of a single-mode fiber. Key characteristics of such multipeak solitons, such as the formation mechanism, propagation stability, and shape-changing collisions, are revealed in detail. Our results show that this multipeak (symmetric or asymmetric) mode could be regarded as a single pulse formed by a nonlinear superposition of a periodic wave and a single-peak (W-shaped or antidark) soliton. In particular, a phase diagram for different types of nonlinear excitations on a continuous wave background, including the unusual multipeak soliton, the W-shaped soliton, the antidark soliton, the periodic wave, and the known breather rogue wave, is established based on the explicit link between exact solution and modulation instability analysis. Numerical simulations are performed to confirm the propagation stability of the multipeak solitons with symmetric and asymmetric structures. Further, we unveil a remarkable shape-changing feature of asymmetric multipeak solitons. It is interesting that these shape-changing interactions occur not only in the intraspecific collision (soliton mutual collision) but also in the interspecific interaction (soliton-breather interaction). Our results demonstrate that each multipeak soliton exhibits the coexistence of shape change and conservation of the localized energy of a light pulse against the continuous wave background.

DOI: 10.1103/PhysRevE.94.042221

I. INTRODUCTION

Nonlinear waves on a continuous wave background in optical fibers have recently become a subject of intense research in both theory and experiment [1–8]. In particular, significant progress has been made in the experimental verification of some unique nonlinear wave structures, including Peregrine rogue waves [9], Kuznetsov-Ma breathers (KMBs) [10], Akhmediev breathers (ABs) [11], as well as their shape-unchanging interactions such as the AB collision [12] and the superregular breather [8,13] (i.e., the quasi-AB collision with a $\pi/2$ phase shift) in the picosecond regime. These picosecond pulses are well described by the standard nonlinear Schrödinger equation (NLSE), which accounts for the second-order dispersion and self-phase modulation. Specifically, these unique waves appear as a result of the modulation instability (MI) [5–8,14], and in turn the common features and differences among wave manifestations enrich the MI understanding of the nonlinear stage. It should be emphasized that a crucial precise link between rogue waves and the zero-frequency MI subregion has recently been unveiled [15,16], although the exact relations between various types of nonlinear waves on a background and MI still remain largely unexplored. On the other hand, the utility of these waves based on their special properties in generating high-quality pulse trains [17], high-power pulses [18], breatherlike solitons [19], nonlinear Talbot effects [20], and the Peregrine comb [21] has been revealed.

In the present work, we extend nonlinear waves on a continuous wave background in the femtosecond regime, since ultrashort pulses are tempting and desirable to improve the capacity of high-bit-rate transmission systems. However, in this case higher-order effects such as higher-order dispersion and self-steepening play an important role and become non-negligible [22–24]. The resulting models of the higher-order NLSE thus describe nonlinear waves on a continuous wave background with higher accuracy than the standard NLSE. Recent studies demonstrated that nonlinear waves on a continuous wave background in the femtosecond regime exhibit structural diversity beyond the reach of the standard NLSE [25–39]; in particular, some interesting types of nonlinear waves on a background have been unveiled that are completely different from the known breathers and rogue waves [31–39]. The underlying mechanism can be qualitatively but quite explicitly interpreted by the corresponding MI features [31,34,35]. Here, we report and discuss a family of multiparametric symmetric and asymmetric multipeak solitons on a continuous wave background in the femtosecond regime. One key characteristic of this soliton is that it exhibits both localization and periodicity along the transverse distribution on a background; the corresponding periodicity and localization for (symmetric or asymmetric) solitons are well described by a periodic wave and a single-peak (W-shaped or antidark) soliton, respectively. We focus our attention in particular on the important properties of these multipeak solitons, including the generation mechanism, propagation stability, and the shape-changing interaction feature of asymmetric multipeak solitons. For special parameter values (the continuous wave background frequency vanishes), part of our general multipeak soliton solution (i.e., the symmetric case) reduces to results reported quite recently [37].

The rest of the paper is structured as follows. In Sec. II, we obtain the exact solution with a unified form describing

*nwudavid@163.com

†zyyang@nwu.edu.cn

symmetric and asymmetric multipeak solitons on a background of the higher-order NLSE. The consistency between the symmetric and asymmetric solitons is revealed by the optical intensity against the background. Section III shows that the periodicity and localization for (symmetric or asymmetric) solitons are well described by a periodic wave and a single-peak (W-shaped or antidark) soliton. In Sec. IV, the phase diagram for different types of nonlinear excitations is presented on the continuous wave frequency and the perturbed frequency plane. Time-efficient numerical simulations were performed to confirm the propagation stability of the multipeak solitons in Sec. V. Section VI unveils the striking shape-changing feature of asymmetric multipeak solitons that occurs not only in the intraspecific collision (soliton mutual collision) but also in the interspecific interaction (soliton-breather interaction). The final section presents our conclusions.

II. THE MODEL AND MULTIPEAK SOLITONS ON A CONTINUOUS WAVE BACKGROUND

Femtosecond pulse (i.e., the duration is shorter than 100 fs) propagation in optical fibers with higher-order physical effects such as third-order dispersion, self-steepening, and delayed nonlinear response is governed by the following higher-order NLSE [22,23]:

$$iu_\xi + \tfrac{1}{2}\alpha u_{\tau\tau} + \gamma|u|^2u - i\beta u_{\tau\tau\tau} - is(|u|^2u)_\tau - i\delta u(|u|^2)_\tau = 0, \tag{1}$$

where u is the envelope of the electric field, ξ is the propagation distance, τ is the retarded time, α and γ are second-order dispersion and self-phase modulation, β is the third-order dispersion, s is the self-steepening coefficient, and δ is the delayed nonlinear response. All quantities have been normalized.

To study nonlinear waves in the femtosecond regime exactly, we shall consider a special parametric condition for the higher-order terms, i.e., $s = 6\beta$, $s + \delta = 0$, with $\alpha = \gamma$. As a result, the model (1) reduces to the integrable Hirota equation [40]. The latter has been studied in a number of papers [27,34,37,40–45], which involve mainly standard bright solitons [41–44], breathers [45], and rogue waves [27]. In contrast to the aforementioned results, we introduce, in the following, an interesting family of multiparametric nonlinear wave solutions describing symmetric and asymmetric multipeak solitons on a continuous wave background in the femtosecond regime.

By means of the Darboux transformation method [46,47], multipeak solitons on a continuous wave background with symmetric and asymmetric amplitude structures can be described by the analytical unified solution with a general and concise form,

$$u_{1,2} = \left[\frac{\Delta_{1,2}\cosh(\varphi+\delta_{1,2}) + \Xi_{1,2}\cos(\phi+\xi_{1,2})}{\Omega_{1,2}\cosh(\varphi+\omega_{1,2}) + \Gamma_{1,2}\cos(\phi+\gamma_{1,2})} + a\right]e^{i\theta}, \tag{2}$$

where the continuous wave background has the following expression: $u_0 = ae^{i\theta}$, $\theta = q\tau + [\alpha a^2 - \alpha q^2/2 + \beta(6qa^2 - q^3)]\xi$, and u_1, u_2 stand for the symmetric and asymmetric multipeak solitons, respectively. It is evident that the solution (2) is formed by a nonlinear superposition of the hyperbolic function $\cosh\varphi$ and the trigonometric function $\cos\phi$ on the background u_0. This unique nonlinear superposition signal exhibits the characteristics of the nonlinear structures on the nonvanishing background, which are expressed as

$$\begin{aligned}
&\varphi = 2\eta_i(\tau + v\xi), \quad \phi = 2\eta_r(\tau + v\xi),\\
&v = \beta\left(2a^2 + 4a_1^2 - q_1^2\right) - (q_1+q)(q\beta + \alpha/2),\\
&\eta_r + i\eta_i = \sqrt{\epsilon + i\epsilon'}, \quad \epsilon = a^2 - a_1^2 + (q-q_1)^2/4,\\
&\epsilon' = a_1(q-q_1), \quad q_1 = -\alpha/(4\beta) - q/2,
\end{aligned} \tag{3}$$

with the corresponding amplitude and phase notations:

$$\begin{aligned}
&\Delta_1 = -4aa_1\sqrt{\rho+\rho'}, \quad \Delta_2 = -4a^2a_1,\\
&\Xi_1 = 2a_1\sqrt{\chi^2 - (2a^2-\chi)^2}, \quad \Xi_2 = 4aa_1\sqrt{2(i\epsilon' - \epsilon)},\\
&\Omega_1 = \rho + \rho', \quad \Omega_2 = \sqrt{\rho^2 - \rho'^2},\\
&\Gamma_1 = -2a(\eta_i + a_1), \quad \Gamma_2 = \sqrt{\varrho^2 + \varrho'^2},\\
&\delta_1 = \operatorname{arctanh}(-i\chi_1/\chi_2),\\
&\delta_2 = \operatorname{arctanh}[i2(\eta_i + i\eta_r)/(q - q_1 - 2ia_1)],\\
&\xi_1 = -\arctan[i(2a^2 - \chi)/\chi],\\
&\xi_2 = -\arctan[i2(\eta_i + i\eta_r)/(q - q_1 - 2ia_1)],\\
&\omega_1 = 0, \quad \omega_2 = \operatorname{arctanh}(-\rho'/\rho),\\
&\gamma_1 = 0, \quad \gamma_2 = -\arctan(\varrho'/\varrho),
\end{aligned}$$

and $\rho = \epsilon + 2a_1^2 + \eta_i^2 + \eta_r^2$, $\rho' = \eta_r(q-q_1) + 2\eta_i a_1$, $\varrho = \epsilon + 2a_1^2 - \eta_i^2 - \eta_r^2$, $\varrho' = \eta_i(q_1 - q) + 2\eta_r a_1$, $\chi = \chi_1^2 + \chi_2^2 + a^2$, $\chi_1 = \eta_r + (q-q_1)/2$, and $\chi_2 = \eta_i + a_1$.

The above expressions depend on the continuous wave background amplitude a, frequency q, the real constant a_1 (without loss of generality we let $a_1 \geqslant 0$), the real parameter α describing the group-velocity dispersion and the self-phase modulation, and the real parameter β (a small value), which is responsible for the higher-order terms. Note that the existence condition $q_1 = -\alpha/(4\beta) - q/2$ [see Eq. (3)] implies that this nonlinear mode is induced by the higher-order effects ($\beta \neq 0$), and therefore it has no analogy in the picosecond regime governed by the standard NLSE. Additionally, the background frequency q plays a key role in the properties of nonlinear modes, since it cannot be ignored by the Galilean transformation. Indeed, the nonlinear modes exhibit prolific structures depending on the value of q (see, e.g., Figs. 1 and 2).

The key property of this solution is that it features both hyperbolic and trigonometric functions with the same velocity v [see the hyperbolic function ($\cosh\varphi$) and the trigonometric function ($\cos\phi$)]. This implies $\eta_r \neq 0, \eta_i \neq 0$ [thus $q \neq q_1$, i.e., $q \neq -\alpha/(6\beta)$]. As a result, the hyperbolic functions and trigonometric functions describe the localization and the periodicity of the transverse distribution τ of the localized waves, respectively. The corresponding typical optical amplitude [$I = \sqrt{|u_{1,2}(\xi,\tau)|^2}$] profiles are well displayed in Fig. 1.

Remarkably, the pulse features a localized solitonlike multipeak structure propagating in the ξ direction. Or, strictly speaking, this interesting solitary mode exhibits both localization and periodicity along the transverse distribution τ. This indicates that the characteristics of this wave come from a mixture of a soliton and a periodic wave. Specifically, this pulse

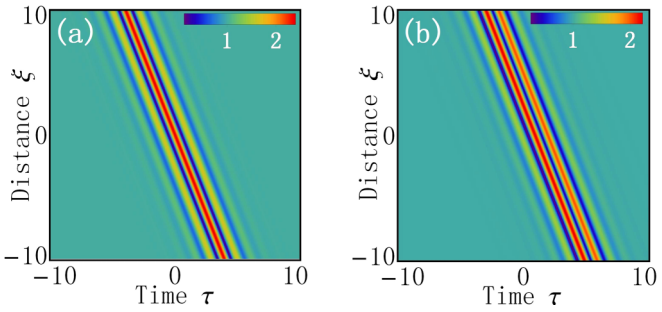

FIG. 1. Optical amplitude distributions $|u|$ of multipeak solitons on a continuous wave background with (a) symmetric u_1 and (b) asymmetric u_2 structures. The setup is $q = 3q_s$, $a = 1$, $a_1 = 0.7$, $\beta = 0.1$, and $\alpha = 1$, with $q_s = -\alpha/(6\beta)$.

possesses a main peak and several subpeaks, and the latter are distributed on both sides of the main peak in a symmetric or asymmetric way. Although the maximum optical intensity is different, the interesting connection is that the optical intensity against the background of the two solitons with symmetric and asymmetric profiles turns out to coincide with each other, i.e., $\int_{-\infty}^{+\infty}(|u_1|^2 - a^2)d\tau = \int_{-\infty}^{+\infty}(|u_2|^2 - a^2)d\tau$. It should be noted that the solution (2) includes, as a special case, the symmetric solution u_1 with $q = 0$ that was reported in Ref. [37].

III. FORMATION MECHANISM FOR MULTIPEAK SOLITONS

Next, to further understand the formation mechanism of the localized multipeak structure on a background, our attention is then focused on extracting separately the periodic wave (periodicity) and soliton (localization) from the mixed state.

Toward that end, the nonlinear excitation signal possesses a single modulated function (hyperbolic or trigonometric functions). In this interesting case, the background frequency q plays a key role and should be chosen as $q = -\alpha/(6\beta)$ (thus $q \neq 0$). Specifically, the periodic wave exists on its own when $\eta_i = 0$ vanishes (thus $a_1 < a$), while the soliton exists in isolation when $\eta_r = 0$ vanishes (thus $a_1 > a$). The unified explicit expressions read, for the periodic wave,

$$u_{p1,2} = \left[\frac{2\eta^2}{a - e^{i\sigma}a_1\cos[2\eta(\tau + v\xi) - \mu]} - a\right]e^{i\theta}, \quad (4)$$

where $\eta = \pm\sqrt{a^2 - a_1^2}$, $\sigma = \sigma_{1,2} = \{0,\pi\}$, with $\mu = \mu_{1,2} = \{0, \arctan(-\eta_r/a_1)\}$, and for the soliton

$$u_{s1,2} = \left[\frac{2\eta'^2}{e^{i\sigma}a_1\cosh[2\eta'(\tau + v\xi) + \mu'] - a} - a\right]e^{i\theta}, \quad (5)$$

where $\eta' = \pm\sqrt{a_1^2 - a^2}$, $\sigma = \sigma_{1,2} = \{0,\pi\}$, with $\mu' = \mu'_{1,2} = \{0, \text{arctanh}(-\eta_i/a_1)\}$.

Figure 2 depicts the typical optical amplitude profiles of the periodic waves and solitons extracted from the localized modes u_1,u_2, respectively. As is shown, the periodic waves possess the same profile feature (the same W-shaped structure of periodic units and the same intensity), but for a slight phase shift. Surprisingly, the single-peak solutions display completely different structures depending on the phases: one is a W-shaped soliton with one peak and two symmetric valleys whose central position is located at $(\xi,\tau) = (0,0)$, extracted from the symmetric multipeak soliton u_1; the another is an antidark soliton (a bright soliton on a nonvanishing background) with a slight phase shift, extracted from the asymmetric multipeak soliton u_2. We note that the optical intensity against the background of the two types of solitons is consistent with each other. It is worth pointing out that the rational W-shaped soliton reported before is only the limiting case of u_{s1} and u_{p1} with $a_1 = a$ [34].

An analysis of the above results, shown in Figs. 1 and 2, implies that a formation mechanism of the localized periodic modes may be interpreted as a nonlinear superposition of a periodic wave and a single-peak soliton. The W-shaped and antidark solitons with periodic modulation give rise to the symmetric and asymmetric multipeak modes, respectively.

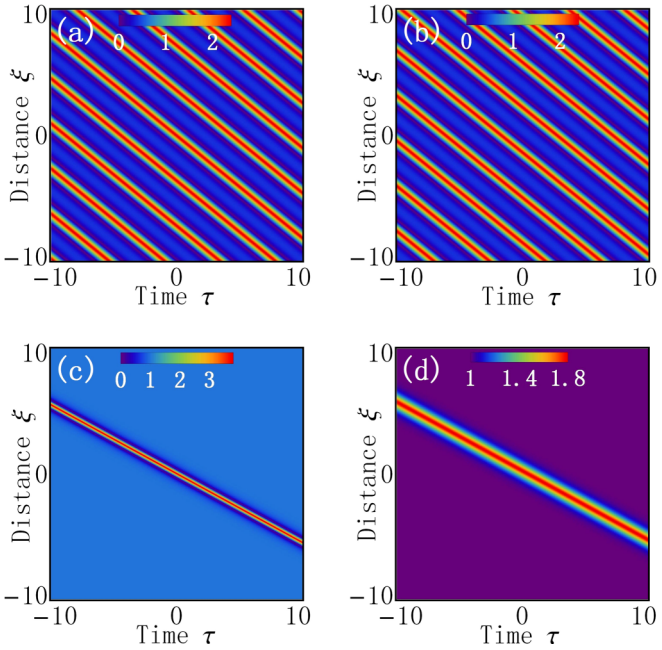

FIG. 2. Periodic waves and single-peak solitons extracted from the multipeak solitons. Periodic waves: (a) u_{p1} and (b) u_{p2} with $a_1 = 0.7$, given by Eqs. (4); single-peak solitons: (c) u_{s1} and (b) u_{s2} with $a_1 = 1.4$, given by Eqs. (5). Other parameters are $a = 1$, $\beta = 0.1$, and $\alpha = 1$.

IV. PHASE DIAGRAM AND TRANSITIONS

A. Phase diagram

The next step of interest and significance is to understand the multipeak structures on a background via MI. Toward that end, we turn our attention first to the standard linear stability analysis of the continuous wave u_0 via adding small-amplitude perturbed Fourier modes p, i.e., $u_p = [a + p]e^{i\theta}$, where $p = f_+e^{i(Q\tau+\omega\xi)} + f_-^*e^{-i(Q\tau+\omega^*\xi)}$, f_+, f_-^* are small amplitudes, Q represents perturbed frequency, and the parameter ω is assumed to be complex. In this case, by comparing the perturbed modes p with the unique exact nonlinear superposition signal in $u_{1,2}$, the nonlinear modes, Eq. (2), shall be regarded as the nonlinear perturbation signal on

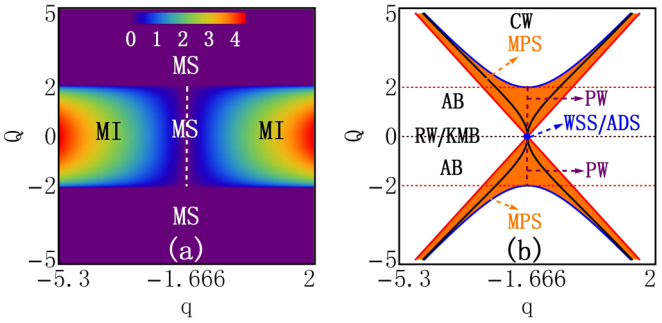

FIG. 3. (a) Characteristics of the modulation instability growth rate on the perturbed frequency and the background frequency (Q,q) plane with higher-order effects, and (b) the explicit correspondence of the phase diagram for different types of nonlinear excitations on a continuous wave background. In (a), the notations "MI" and "MS" denote modulation instability and modulation stability regions, respectively. In (b), "RW" (Peregrine rogue wave), "KMB" (Kuznetsov-Ma breather), and "AB" (Akhmediev breather) are cast in the MI region with corresponding exact perturbed frequencies $Q=0$, $Q=0$, and $|Q|<2a$ $(Q\neq 0)$, respectively. "WSS" (W-shaped soliton), "ADS" (antidark soliton), and "PW" (periodic wave) are mapped in the MS line $q=q_s$; specifically, W-shaped and antidark solitons exist at $(q,Q)=(q_s,0)$ (the blue dot), and periodic waves exist at $q=q_s$ with $|Q|\leqslant 2a$ $(Q\neq 0)$. The "MPS" (multipeak soliton), whether the structure is symmetric or asymmetric, is displayed in the same orange "X-shaped" region, which is depicted via the explicit perturbed frequency expression $2\eta_r$ with different values of a_1, from $a_1=0$ to $a_1\gg a$. Here the solid blue, black, and red lines in the orange region correspond to the cases with $a_1=0$, $a_1=a$, and $a_1\gg a$, respectively. The setup is $\beta=0.1$, $\alpha=1$, and $a=1$.

background u_0 with the explicit perturbed frequency $Q=2\eta_r$. Different perturbed frequencies correspond to different types of nonlinear excitations [48]. In this regard, we can establish an explicit correspondence between various nonlinear excitations and MI on the (Q,q) plane. The corresponding characteristic outcomes are displayed in Fig. 3.

Figure 3(a) depicts the typical characteristics of MI growth rate $G=-\mathrm{Im}\{\omega\}$, and Fig. 3(b) shows the explicit correspondence between MI and various nonlinear excitations. Remarkably, there is a modulation stability (MS) region [dashed line in Fig. 3(a)], i.e., $G=0$, in the low perturbed frequency region $(|Q|\leqslant 2a)$, resulting from the higher-order effects, which is given analytically by $q=q_s=-\alpha/(6\beta)$. Hence MI is always present in the region $|Q|\leqslant 2a$ $(q\neq q_s)$. Instead, the MS regions contain the whole higher perturbation frequency region $(|Q|>2a)$ and a special MS region $q=q_s$ in a low perturbation frequency region $(|Q|\leqslant 2a)$.

An interesting finding is that the MS condition $q=q_s$ is consistent with the existence condition of a periodic wave and a single-peak soliton, Eqs. (4) and (5). According to their perturbed frequencies, the W-shaped/antidark solitons are located at $(q,Q)=(q_s,0)$, and periodic waves exist at the $q=q_s$ line with $|Q|<2a, Q\neq 0$.

Next, we map the whole distribution region of multipeak solitons on the MI plane. Toward that end, the modulated parameter a_1 of the perturbed frequency $2\eta_r$ is considered as a continuous variable from $a_1=0$ to $a_1\gg a$. The corresponding marginal condition can be found analytically: $Q=\pm\{4a^2+9\Lambda^2/4\}^{1/2}$ (when $a'=0$ with $\Lambda=q-q_s$), $Q=\pm 3|\Lambda|/2$ (when $a_1\gg a$). Thus, the existence range of the multipeak solitons is identified in the orange "X-shaped" region between the two marginal lines [see Fig. 3(b)].

Remarkably, this unique "X-shaped" region involves both a MS subregion with higher perturbation frequency $(|Q|>2a)$ and a MI subregion with low perturbation frequency $(|Q|<2a)$. Further, the solid black line in the "X-shaped" region represents the intermediate condition with $a_1=a$, which can be given analytically as $Q=\pm\{[(9\Lambda^2/8)^2+9a^2\Lambda^2]^{1/2}+9\Lambda^2/8\}^{1/2}$. It is interesting to note that, if $q=q_s$, the region $a_1\geqslant a$ [i.e., the range from red line to black line] reduces to the point $(q,Q)=(q_s,0)$, where multipeak solitons are converted into W-shaped/antidark solitons, while another region $0\leqslant a_1<a$ [i.e., the range from black line to blue line] reduces to the $q=q_s$ line with $|Q|\leqslant 2a, Q\neq 0$, where multipeak solitons are translated into periodic waves. We stress that this finding coincides with the transition condition for nonlinear waves in Eqs. (4) and (5).

B. Transitions

On the other hand, it is also worth pointing out that the generation mechanism of the periodic waves and W-shaped/antidark solitons can be interpreted as the transitions when the AB and KMB evolve and reach the MS region $q=q_s$, respectively. This can be anticipated visually by the phase diagram above, and proved strictly via the general exact AB and KMB solutions with different phases $(\sigma=0,\pi)$ presented in the Appendix. Specifically, as $q\to q_s$, the AB has its ξ-direction localization gradually decreasing, which corresponds exactly to the MI growth rate attenuation. The AB is eventually translated into the periodic wave with the vanishing growth rate, i.e., $q=q_s$. Please note that the different phase parameters have no substantial influence on the AB-to-periodic wave transition (see Fig. 4). For the KMB, its breathing period $D_\xi=\pi/[\eta' a_1\alpha(1-q/q_s)]$ increases, and the fundamental unit becomes more elongated as $q\to q_s$ (see Fig. 5). It is noteworthy to observe KMB-to-W-shaped/antidark soliton transitions resulting from the KMBs with different phase parameters. The KMB can be transformed into a W-shaped soliton when $\sigma=0$ [its peak is located at the central position $(\xi,\tau)=(0,0)$], whereas it becomes an antidark soliton on the MS line.

V. STABILITY FOR MULTIPEAK SOLITONS

As is well known, the stability plays an irreplaceable role in nonlinear wave realization and application in experiment. On the other hand, one should keep in mind that the multipeak solitons reported above are on a continuous wave background. The latter, in general, displays the feature of MI, namely, a small perturbation may distort the wave profiles formed on top of it. In this regard, we shall test the stability of multipeak soliton propagation on a continuous wave background. We perform direct numerical simulations of Eq. (1) by the split-step Fourier method with the initial condition $u_{1,2}(0,\tau)$, i.e., the exact solution (2) at $\xi=0$.

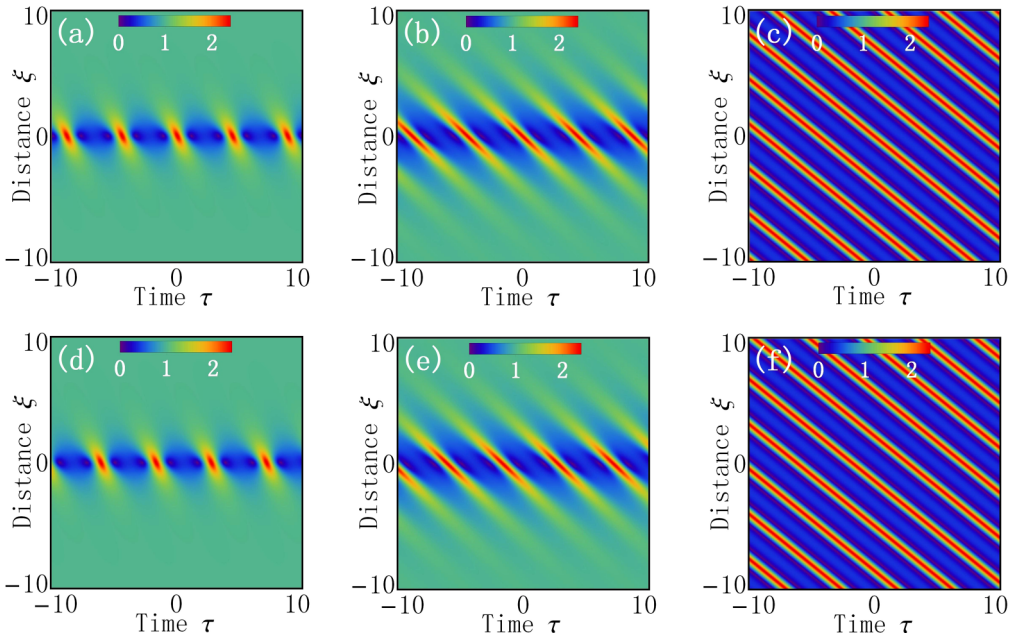

FIG. 4. Transitions from the Akhmediev breathers to the periodic waves with $q = 0$, $q_s/2$, and q_s, from left to right. Top and bottom rows display the modes with different phases $\sigma = 0,\pi$. Other parameters are $a = 1$, $\beta = 0.1$, and $a_1 = 0.7$.

Nevertheless, it should be pointed out that the analytical solution (2) $u_{1,2}$ obtained here is confined to the case with special parameters, i.e., the Hirota model. Thus, it is crucial to conform the sensitivity of the exact solution. Toward that end, we numerically simulate the evolution of the multipeak solitons under the condition departing from the validity of the Hirota case. Namely, we choose the condition $s + \delta = 0$, $s = (6 + \varepsilon)\beta$, with $\varepsilon \ll 1$, which is beyond the Hirota case. Figures 6 and 7 show the stability of the symmetric and asymmetric multipeak solitons by comparing the analytical solution (2) $u_{1,2}$ with the numerical simulations of Eq. (1).

In Fig. 6, we first show the propagation stability of a typical symmetric multipeak soliton u_1 with $\varepsilon = 0$ and 0.1. Interestingly, our results indicate no collapse arising from the MI, numerical deviations, and in particular the unavailability of the Hirota condition. Instead, stable propagation over tens of propagation distances is observed. In particular, we compare the numerical results with the analytical solution by the corresponding amplitude profiles at different ξ. It shows in

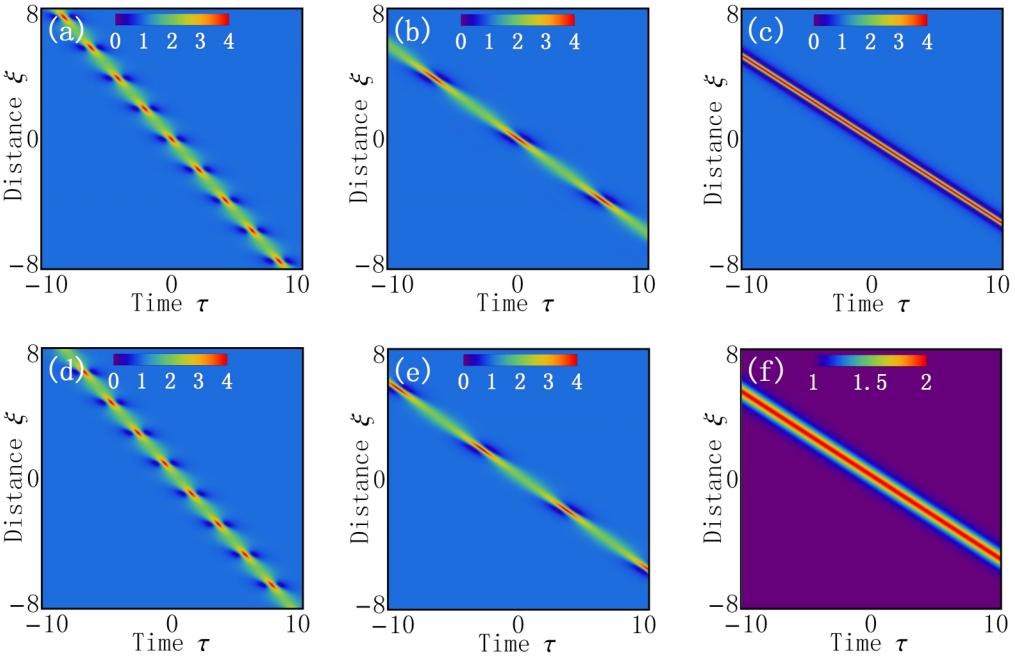

FIG. 5. Transitions from the Kuznetsov-Ma breathers to the single-peak solitons with $q = 0$, $q_s/2$, and q_s, from left to right. Top and bottom rows display the localized modes with different phases $\sigma = 0,\pi$. Other parameters are $a = 1$, $\beta = 0.1$, and $a_1 = 1.5$.

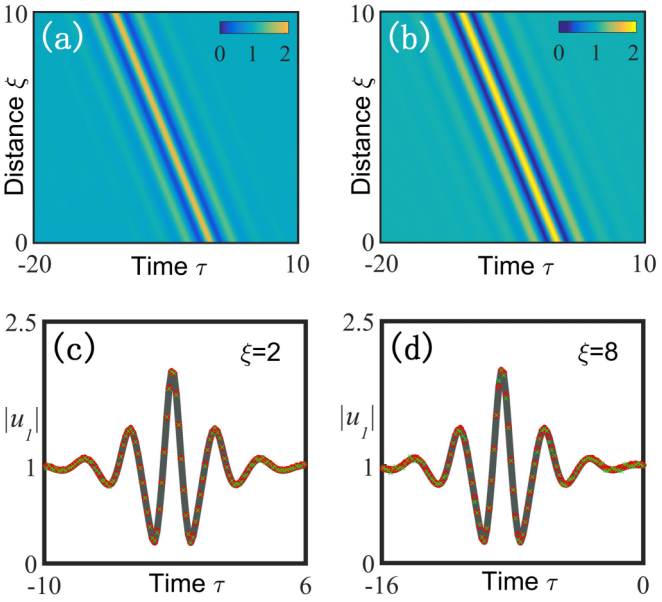

FIG. 6. Numerical stability confirmation for the symmetric multipeak solitons $|u_1(\xi,\tau)|$ with (a) $\varepsilon = 0$, i.e., the Hirota case, and (b) $\varepsilon = 0.1$. Parts (c) and (d) show the comparison of amplitude profiles of the analytical solution (black solid line), the numerical result in (a) (red circle), and the numerical result in (b) (green cross) at $\xi = 2,8$. The setup is $q = 3q_s/2$, $a = 1$, $\alpha = 1$, $\beta = 0.1$, and $a_1 = 0.5$.

Figs. 6(c) and 6(d) that the numerical results (red circle and green cross) are in good agreement with the analytical solution (solid line).

Next, we test the stability of the asymmetric multipeak soliton. Here, we keep the same parameters as in Fig. 6, but the initial state is chosen as $u_2(0,\tau)$. As shown in Fig. 7, we observe that the asymmetric multipeak soliton can also propagate in a stable manner. Namely, the asymmetric feature

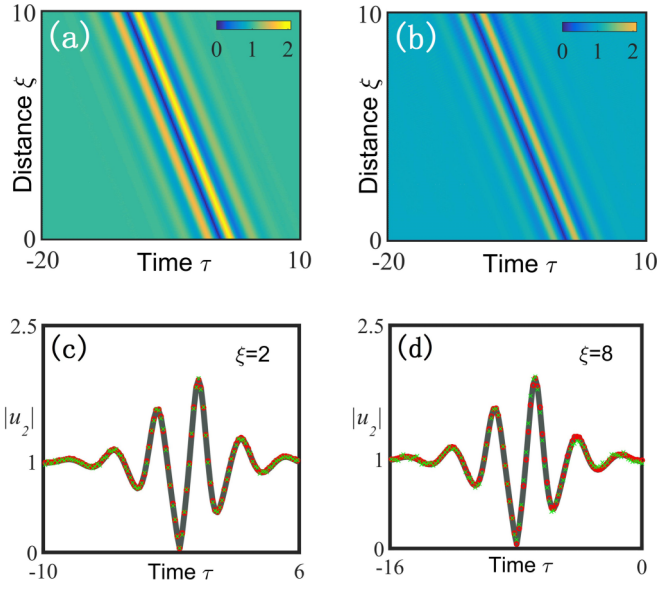

FIG. 7. Numerical stability confirmation for the asymmetric multipeak solitons $|u_2(\xi,\tau)|$. The setup is the same as in Fig. 6, but the initial state is $u_2(0,\tau)$.

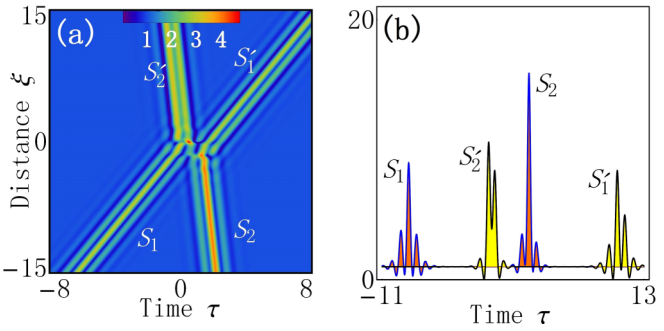

FIG. 8. (a) Shape-changing collision between two multipeak solitons (incident solitons S_1, S_2; the outgoing solitons S_1', S_2') with the conditions $q_j = (3q_s - q)/2, q \neq q_s, j = 1,2$. (b) The corresponding intensity profiles $|u|^2$ at $\xi = -20$ (orange) and $\xi = 20$ (yellow). The setup is $q = 4q_s$, $a_1 = 1$, $a_2 = 1.5$, $a = 1$, $\alpha = 1$, and $\beta = 0.1$.

of the transverse amplitude distribution seems to have no effect on the propagation stability of the multipeak solitons. It should be pointed out that although here we have demonstrated the results of the stability only for the multipeak solitons in Eq. (1), similar conclusions hold for other types of nonlinear waves as well, provided propagation distances are kept within reasonable values.

VI. SHAPE-CHANGING FEATURE OF ASYMMETRIC MULTIPEAK SOLITONS

In this section, we focus our attention on the characteristics of the interaction between nonlinear waves reported above. In fact, we find that rich intraspecific and interspecific interactions do exist in this system via extracting explicit existence conditions from Table I in the Appendix. However, our interest is confined to a different kind of shape-changing interaction. Specifically, we find that the asymmetric multipeak soliton u_2 exhibits shape-changing characteristics before and after interactions. Interestingly, this shape-changing interaction involves mutual collisions of multipeak solitons as well as interactions between multipeak solitons and other types of nonlinear waves. In particular, it is found that the shape-changing feature is specific to the multipeak solitons.

We first study the mutual collision of two multipeak solitons with the coexistence condition $q_j = (3q_s - q)/2$, $q \neq q_s$, $j = 1,2$. As shown in Fig. 8, two incident multipeak solitons S_1, S_2 with different features of peak distributions move from $\xi \to -\infty$ and approach each other; they undergo collision around $(\xi,\tau) = (0,0)$ and form a higher peak. They then separate with a small phase shift and propagate to $\xi \to +\infty$. It is evident that the multipeak features of outgoing multipeak structures S_1', S_2', including the peak numbers and peak intensity distributions, are changed significantly after the collision (see the intensity profiles in Fig. 8). This indicates that the collision is shape-changing. For details, by comparing the intensity profiles S_1, S_2 with S_1', S_2', we find that, for each soliton, the maximum intensity decreases while the subpeaks increase. We infer that this fascinating shape-changing collision could stem from the intensity transfer from subpeaks to main peaks of the multipeak soliton itself, rather than the intensity transfer between solitons.

To prove the validity of the conjecture above, we then analyze the localized energy of a light pulse against the background of multipeak solitons with the expression $I_e = \int_{\tau_1}^{\tau_2} \{|u(\xi,\tau)|^2 - a^2\} d\tau$. As a result, the localized energy of multipeak solitons before and after the shape-changing collision can be investigated via the optimal numerical method at different propagation distances ξ. The total localized energy of these two solitons $[I_e(s_1) + I_e(s_2)]$ is conserved, which can be verified directly when $\tau_1 = -\infty, \tau_2 = +\infty$. The localized energy of the each multipeak soliton $[I_e(s_1), I_e(s_2)]$ is obtained by the appropriate choice for τ_1, τ_2. For a selected initial propagation distance, i.e., $\xi < 0$, we calculate $I_e(s_1)$ and $I_e(s_2)$ by $\int_{-\infty}^{\tau_0} \{|u|^2 - a^2\} d\tau$ and $\int_{\tau_0}^{+\infty} \{|u|^2 - a^2\} d\tau$, respectively. Note that the transverse position τ_0 is located between S_1, S_2, leading to $|u(\xi,\tau_0)| = a$, and vice versa for positive ξ. Then the interesting finding is that each multipeak soliton preserves its localized energy before and after the collision. Namely, after multipeak solitons collide, the shape change and localized energy conservation of each multipeak soliton coexist. It is noted that this shape-changing feature is completely different from the known shape-changing collisions between standard solitons in the coupled NLS systems that describe a process of energy transference between solitons in one component [49].

For a better understanding of this shape-changing characteristic of multipeak solitons, we next explore interspecific interactions, i.e., the interactions between multipeak solitons and other types of localized nonlinear waves (breathers). Our aim is to demonstrate that after the interspecific interaction occurs, the multipeak solitons exhibit intensity redistribution, but the characteristic of breathers remains invariant.

Figure 9 illustrates the interaction between multipeak solitons and breathers for the choice of the parameters $q_1 = (3q_s - q)/2$, $q \neq q_s$, $q_2 \neq (3q_s - q)/2$. One can see from Fig. 9 that an incident multipeak soliton S propagating along ξ collides with a breather near $\xi = 0$; after that, the outgoing soliton S' shows a typical shape-changing characteristic, but the breather remains the original feature. An analysis of the intensity profiles and the localized energy of S and S' shows that, after the interspecific interaction with a breather occurs, the single multipeak soliton allows the intensity redistribution between their peaks, and preserves strictly the localized energy of the soliton.

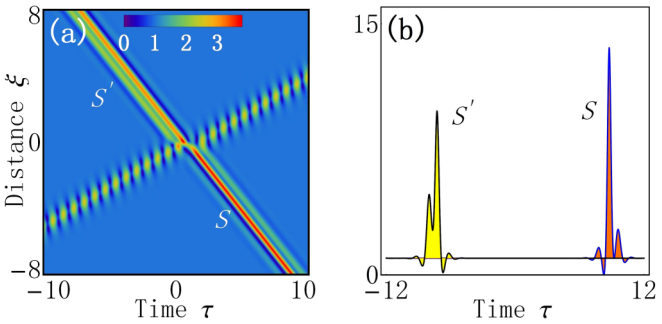

FIG. 9. (a) Shape-changing interaction between a breather and a multipeak soliton (the incident soliton S and breather B; the outgoing soliton S' and breather B') with the conditions $q_1 = (3q_s - q)/2, q \neq q_s; q_2 \neq (3q_s - q)/2$. (b) The corresponding intensity profiles $|u|^2$ of multipeak solitons at $\xi = -8$ (orange) and $\xi = 8$ (yellow). The setup is $q = 3q_s, a_1 = 1.4, a_2 = 0.8, q_2 = 1.6, a = 1, \alpha = 1$, and $\beta = 0.1$.

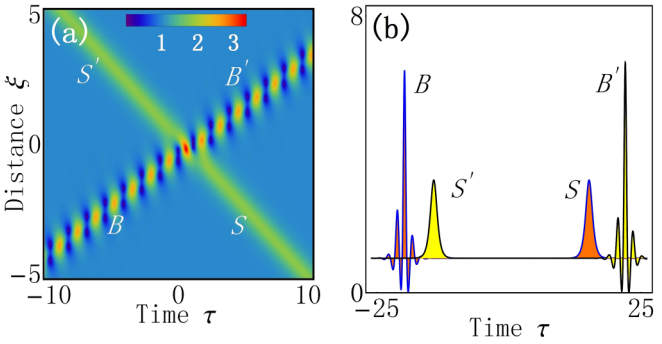

FIG. 10. (a) Shape-unchanging interaction between a breather and an antidark soliton (the incident soliton S and breather B; the outgoing soliton S' and breather B') with the conditions $q_1 = (3q_s - q)/2, q = q_s, a_1^2 > a^2; q_2 \neq (3q_s - q)/2$. (b) The corresponding intensity profiles $|u|^2$ at $\xi = -8$ (orange) and $\xi = 8$ (yellow). The setup is the same as in Fig. 9, but $q = q_s$.

Finally, we illuminate that the unique shape-changing characteristic is specific to the multipeak solitons. Toward that end, we consider the limiting case of the interaction shown in Fig. 9, i.e., the collision between antidark solitons and breathers. The corresponding interaction structure is displayed in Fig. 10 with the limiting condition $q = q_s$. It is evident that this collision exhibits a completely shape-unchanging feature, although the waves are two distinct types of localized waves. As a result, a comparison of Figs. 9 and 10 indicates that the shape-changing feature is specific to asymmetric multipeak solitons and is not available for antidark solitons.

VII. CONCLUSION

In summary, symmetric and asymmetric multipeak solitons on a continuous wave background in the femtosecond regime have been investigated analytically and numerically. Key properties of such multipeak solitons as the formation mechanism, propagation stability, and shape-changing collisions have been revealed in detail.

This intriguing multipeak soliton exhibits both localization and periodicity along the transverse distribution on a background. The corresponding periodicity and localization for multipeak (symmetric or asymmetric) solitons are well described by a periodic wave and a single-peak (W-shaped or antidark) soliton, respectively.

Although the maximum optical intensity is different, the interesting connection is that the optical intensity against the background of the symmetric and asymmetric solitons turns out to coincide under the same initial parameter condition, i.e., $\int_{-\infty}^{+\infty} (|u_1|^2 - a^2) d\tau = \int_{-\infty}^{+\infty} (|u_2|^2 - a^2) d\tau$.

In particular, a phase diagram for different types of nonlinear excitations on a continuous wave background, including a breather, a rogue wave, a W-shaped soliton, an antidark soliton, a periodic wave, and a multipeak soliton, is established based on the explicit link between the exact nonlinear wave solution and MI analysis. Numerical simulations were performed to confirm the propagation stability of the multipeak solitons.

Finally, the remarkable shape-changing feature of asymmetric multipeak solitons, occurring not only in the intraspecific collision (soliton mutual collision) but also in the interspecific interaction (soliton-breather interaction), was

unveiled. It is demonstrated that each multipeak soliton exhibits the coexistence of shape change and conservation of the localized energy of a light pulse against the continuous wave background. The shape-changing interaction between nonlinear waves on a continuous wave background will enrich our understanding of localized wave collision in (1+1)-dimensional scalar nonlinear wave evolution systems.

ACKNOWLEDGMENTS

This work has been supported by the National Natural Science Foundation of China (NSFC) (Grants No. 11475135, No. 11547302, No. 61505101, No. 11434013, and No. 11425522). We are grateful to Q. Guo (South China Normal University) for his valuable comments at NSOS (Nov. 6–8, 2015). C.L. also thanks F. Baronio for his helpful suggestion, and Fa-kai Wen and Wen-Hao Xu for helpful discussions.

APPENDIX

A general nonlinear wave solution on the background u_0 of the higher-order NLSE (1), which describes optical femtosecond pulse propagation in a single-mode fiber, is present as follows:

$$u_{1,2}=\left[\frac{\Delta_{1,2}\cosh(\varphi+\delta_{1,2})+\Xi_{1,2}\cos(\phi+\xi_{1,2})}{\Omega_{1,2}\cosh(\varphi+\omega_{1,2})+\Gamma_{1,2}\cos(\phi+\gamma_{1,2})}+a\right]e^{i\theta}, \tag{A1}$$

where

$$\begin{aligned}
&\varphi=2\eta_i(\tau+V_1\xi),\quad \phi=2\eta_r(\tau+V_2\xi),\\
&V_1=v_1+v_2\eta_r/\eta_i,\quad V_2=v_1-v_2\eta_i/\eta_r,\\
&v_1=\beta\left(2a^2+4a_1^2-q'^2\right)-(q_1+q)(q\beta+\alpha/2),\\
&v_2=a_1[\alpha+2\beta(q+2q_1)],\quad \eta_r+i\eta_i=\sqrt{\epsilon+i\epsilon'},\\
&\epsilon=a^2-a_1^2+(q-q_1)^2/4,\quad \epsilon'=a_1(q-q_1).
\end{aligned}$$

TABLE I. Types of nonlinear excitations and corresponding explicit existence conditions.

Nonlinear wave type	Existence condition
Breather and rogue wave	$q_j\neq\frac{3q_s-q}{2}$ $(q_s=\frac{-\alpha}{6\beta},j=1,2)$
Multipeak soliton	$q_j=\frac{3q_s-q}{2},q\neq q_s$
W-shaped/antidark soliton	$q_j=\frac{3q_s-q}{2},q=q_s,a^2<a_j^2$
Periodic wave	$q_j=\frac{3q_s-q}{2},q=q_s,a^2>a_j^2$
Rational W-shaped soliton	$q_j=\frac{3q_s-q}{2},q=q_s,a^2=a_j^2$

Here we remark that if $V_1=V_2$, implying $v_2=0$ [thus $q_1=-\alpha/(4\beta)-q/2$], the solution (A1) describes the dynamics of multipeak solitons in Eq. (2). Instead, if $V_1\neq V_2$, implying $v_2\neq 0$, the solution (A1) displays the properties of the breather and the rogue wave. Specifically, with the condition $0<a_1<a,q=q_1$, the Akhmediev breather solution is given by the form

$$u_{1,2}=\left[\frac{2\eta^2\cosh(\kappa\xi)+i2\eta a_1\sinh(\kappa\xi)}{a\cosh(\kappa\xi)-e^{i\sigma}a_1\cos[2\eta(\tau+v_1\xi)-\mu]}-a\right]e^{i\theta}, \tag{A2}$$

where $v_1=\beta(2a^2+4a_1^2-q^2)-2q(q\beta+\alpha/2)$, $\kappa=2\eta v_2$, $v_2=a_1\alpha(1-q/q_s)$, $q_s=-\alpha/(6\beta)$, and $\sigma=\sigma_{1,2}=\{0,\pi\}$, with $\mu=\mu_{1,2}=\{0,\arctan(-\eta_r/a_1)\}$. The AB is periodic along the distribution direction τ, and the period is $D_\tau=\pi/\sqrt{a^2-a_1^2}$. On the other hand, the Kuznetsov-Ma breather is obtained with the condition $a_1>a,q=q_1$,

$$u_{1,2}=\left[\frac{2\eta'^2\cos(\kappa'\xi)+i2\eta' a_1\sin(\kappa'\xi)}{e^{i\sigma}a_1\cosh[2\eta'(\tau+v_1\xi)+\mu']-a\cos(\kappa'\xi)}-a\right]e^{i\theta}, \tag{A3}$$

where $\kappa'=2\eta' v_2$, $\sigma=\sigma_{1,2}=\{0,\pi\}$, with $\mu'=\mu'_{1,2}=\{0,\operatorname{arctanh}(-\eta_i/a_1)\}$. Note that if $q=q_s$, the AB and KMB are converted to the periodic wave and W-shaped/antidark soliton described by Eqs. (4) and (5). For clarity, various types of nonlinear excitations extracted from the general solution on a background are classified in Table I.

[1] N. Akhmediev and A. Ankiewicz, *Solitons: Nolinear Pulses and Beams* (Chapman and Hall, London, 1997).
[2] D. R. Solli, C. Ropers, P. Koonath, and B. Jalali, Nature (London) **450**, 1054 (2007).
[3] G. P. Agrawal, J. Opt. Soc. Am. B **28**, A1 (2011).
[4] N. Akhmediev, J. M. Dudley, D. R. Solli, and S. K. Turitsyn, J. Opt. **15**, 060201 (2013).
[5] M. Onorato, S. Residori, U. Bortolozzo, A. Montina, and F. T. Arecchi, Phys. Rep. **528**, 47 (2013).
[6] J. M. Dudley, F. Dias, M. Erkintalo, and G. Genty, Nat. Photon. **8**, 755 (2014).
[7] N. Akhmediev, J. M. Soto-Crespo, and A. Ankiewicz, Phys. Lett. A **373**, 2137 (2009); N. Akhmediev, A. Ankiewicz, and M. Taki, *ibid.* **373**, 675 (2009); N. Akhmediev, J. M. Soto-Crespo, and A. Ankiewicz, Phys. Rev. A **80**, 043818 (2009).
[8] V. E. Zakharov and A. A. Gelash, Phys. Rev. Lett. **111**, 054101 (2013).
[9] D. H. Peregrine, J. Aust. Math. Soc. Ser. B **25**, 16 (1983); B. Kibler, J. Fatome, C. Finot, G. Millot, F. Dias, G. Genty, N. Akhmediev, and J. M. Dudley, Nat. Phys. **6**, 790 (2010).
[10] E. A. Kuznetsov, Sov. Phys. Dokl. **22**, 507 (1977); Y. C. Ma, Stud. Appl. Math. **60**, 43 (1979); B. Kibler, J. Fatome, C. Finot, G. Millot, G. Genty, B. Wetzel, N. Akhmediev, F. Dias, and J. M. Dudley, Sci. Rep. **2**, 463 (2012).
[11] N. Akhmediev and V. I. Korneev, Theor. Math. Phys. **69**, 1089 (1986); J. M. Dudley, G. Genty, F. Dias, B. Kibler, and N. Akhmediev, Opt. Express **17**, 21497 (2009).
[12] B. Frisquet, B. Kibler, and G. Millot, Phys. Rev. X **3**, 041032 (2013).

[13] B. Kibler, A. Chabchoub, A. Gelash, N. Akhmediev, and V. E. Zakharov, Phys. Rev. X **5**, 041026 (2015).
[14] V. E. Zakharov and L. A. Ostrovsky, Physica D **238**, 540 (2009).
[15] F. Baronio, M. Conforti, A. Degasperis, S. Lombardo, M. Onorato, and S. Wabnitz, Phys. Rev. Lett. **113**, 034101 (2014).
[16] F. Baronio, S. Chen, P. Grelu, S. Wabnitz, and M. Conforti, Phys. Rev. A **91**, 033804 (2015).
[17] J. Fatome, B. Kibler, and C. Finot, Opt. Lett. **38**, 1663 (2013).
[18] G. Y. Yang, L. Li, S. T. Jia, and D. Mihalache, Rom. Rep. Phys. **65**, 902 (2013); **65**, 391 (2013).
[19] G. Y. Yang, Y. Wang, Z. Y. Qin, B. A. Malomed, D. Mihalache, and L. Li, Phys. Rev. E **90**, 062909 (2014).
[20] Y. Zhang, M. R. Belić, H. Zheng, H. Chen, C. Li, J. Song, and Y. Zhang, Phys. Rev. E **89**, 032902 (2014); Y. Zhang, M. R. Belić, M. S. Petrović, H. Zheng, H. Chen, C. Li, K. Lu, and Y. Zhang, *ibid.* **91**, 032916 (2015).
[21] C. G. L. Tiofack, S. Coulibaly, M. Taki, S. De Bièvre, and G. Dujardin, Phys. Rev. A **92**, 043837 (2015).
[22] Y. Kodama and A. Hasegawa, IEEE J. Quantum Electron. **23**, 510 (1987).
[23] G. P. Agrawal, *Nonlinear Fiber Optics*, 4th ed. (Academic, Boston, 2007).
[24] J. Yang, *Nonlinear Waves in Integrable and Nonintegrable Systems* (SIAM, Philadelphia, 2010).
[25] A. Ankiewicz, N. Devine, and N. Akhmediev, Phys. Lett. A **373**, 3997 (2009); A. Ankiewicz, J. M. Soto-Crespo, M. A. Chowdhury, and N. Akhmediev, J. Opt. Soc. Am. B **30**, 87 (2013).
[26] U. Bandelow and N. Akhmediev, Phys. Rev. E **86**, 026606 (2012); Phys. Lett. A **376**, 1558 (2012); J. Opt. **15**, 064006 (2013); S. Chen, Phys. Rev. E **88**, 023202 (2013); J. M. Soto-Crespo, N. Devine, N. P. Hoffmann, and N. Akhmediev, *ibid.* **90**, 032902 (2014).
[27] A. Ankiewicz, J. M. Soto-Crespo, and N. Akhmediev, Phys. Rev. E **81**, 046602 (2010); G. Y. Yang, L. Li, and S. T. Jia, *ibid.* **85**, 046608 (2012); Y. S. Tao and J. S. He, *ibid.* **85**, 026601 (2012).
[28] L. H. Wang, K. Porsezian, and J. S. He, Phys. Rev. E **87**, 053202 (2013).
[29] A. Ankiewicz, Y. Wang, S. Wabnitz, and N. Akhmediev, Phys. Rev. E **89**, 012907 (2014).
[30] A. Chowdury, D. J. Kedziora, A. Ankiewicz, and N. Akhmediev, Phys. Rev. E **90**, 032922 (2014).
[31] L. C. Zhao, S. C. Li, and L. M. Ling, Phys. Rev. E **89**, 023210 (2014).
[32] J. S. He, S. W. Xu, M. S. Ruderman, and R. Erdélyi, Chin. Phys. Lett. **31**, 010502 (2014).
[33] L. C. Zhao, Z. Y. Yang, and L. M. Ling, J. Phys. Soc. Jpn. **83**, 104401 (2014).
[34] C. Liu, Z. Y. Yang, L. C. Zhao, and W. L. Yang, Phys. Rev. E **91**, 022904 (2015).
[35] C. Liu, Z. Y. Yang, L. C. Zhao, and W. L. Yang, Ann. Phys. (N.Y.) **362**, 130 (2015).
[36] A. Chowdury, D. J. Kedziora, A. Ankiewicz, and N. Akhmediev, Phys. Rev. E **91**, 022919 (2015).
[37] A. Chowdury, A. Ankiewicz, and N. Akhmediev, Proc. R. Soc. London, Ser. A **471**, 0130 (2015).
[38] L. Wang, J. H. Zhang, Z. Q. Wang, C. Liu, M. Li, F. H. Qi, and R. Guo, Phys. Rev. E **93**, 012214 (2016).
[39] T. Xu, D. Wang, M. Li, and H. Liang, Phys. Scr. **89**, 075207 (2014).
[40] R. Hirota, J. Math. Phys. **14**, 805 (1973).
[41] M. Lakshmanan and S. Ganesan, J. Phys. Soc. Jpn. **52**, 4031 (1983).
[42] D. Mihalache, L. Torner, F. Moldoveanu, N.-C. Panoiu, and N. Truta, Phys. Rev. E **48**, 4699 (1993); D. Mihalache, N.-C. Panoiu, F. Moldoveanu, and D.-M. Baboiu, J. Phys. A **27**, 6177 (1994); D. Mihalache, N. Truta, and L. C. Crasovan, Phys. Rev. E **56**, 1064 (1997).
[43] K. Porsezian and K. Nakkeeran, Phys. Rev. Lett. **76**, 3955 (1996).
[44] J. Yang, Phys. Rev. Lett. **91**, 143903 (2003).
[45] L. Li, Z. Li, Z. Xu, G. Zhou, and K. H. Spatschek, Phys. Rev. E **66**, 046616 (2002); Z. Y. Xu, L. Li, Z. H. Li, and G. S. Zhou, *ibid.* **67**, 026603 (2003); S. Q. Li, L. Li, Z. H. Li, and G. S. Zhou, J. Opt. Soc. Am. B **21**, 2089 (2004).
[46] B. L. Guo, L. M. Ling, and Q. P. Liu, Phys. Rev. E **85**, 026607 (2012).
[47] A. Degasperis and S. Lombardo, Phys. Rev. E **88**, 052914 (2013).
[48] L. C. Zhao and L. M. Ling, J. Opt. Soc. **33**, 850 (2016).
[49] T. Kanna and M. Lakshmanan, Phys. Rev. Lett. **86**, 5043 (2001); Phys. Rev. E **67**, 046617 (2003); M. Vijayajayanthi, T. Kanna, and M. Lakshmanan, Phys. Rev. A **77**, 013820 (2008); S. Rajendran, M. Lakshmanan, and P. Muruganandam, J. Math. Phys. **52**, 023515 (2011); T. Kanna, K. Sakkaravarthi, and M. Vijayajayanthi, Pramana-J. Phys. **85**, 881 (2015).